THE JOURNAL OF PHYSICAL CHEMISTRY C
A JOURNAL OF THE AMERICAN CHEMICAL SOCIETY

pubs.acs.org/JPCC

Article

Vibrational Spectroscopic Analysis of 1,3-Dianiline Squarate: Infrared, Normal Raman, Surface-Enhanced Raman Scattering, and Density Functional Theory Calculations

Vanessa End de Oliveira,* Antônio Rodrigues da Cunha, Márcia de Almeida Rizzutto, Maria Teresa Lamy, Luiz Fernando Cappa de Oliveira, and Erix Alexander Milán-Garcés*

Cite This: J. Phys. Chem. C 2023, 127, 421−428

Read Online

ACCESS | Metrics & More | Article Recommendations | Supporting Information

ABSTRACT: 1,3-Dianiline squarate (DSQ) is an interesting squaraine frequently used as an intermediary reactant in organic synthesis aiming products 1,3-(R_1R_2)-squarate type, as well as a building block of photoinitiators under visible light widely used in photopolymerization reactions. In this work, structural investigations of DSQ were performed using spectroscopic methods such as solid-state 13C nuclear magnetic resonance and several vibrational techniques. Therefore, a detailed vibrational spectroscopic analysis of DSQ was carried out by infrared, normal Raman, and surface-enhanced Raman scattering (SERS) combined with density functional theory calculations. SERS data suggest two preferential interactions between squaraine and the silver nanoparticle. It is proposed that squaraine is adsorbed mainly through a regular Ag−O interaction involving the carbonyl group; that connection impacts the oscillators around them and consequently their vibrational spectra. In addition, the silver atoms may perturb the DSQ planarity by interacting with the phenyl rings; they promote the molecule to adopt a non-planar tilted orientation on the metal nanoparticle surface.

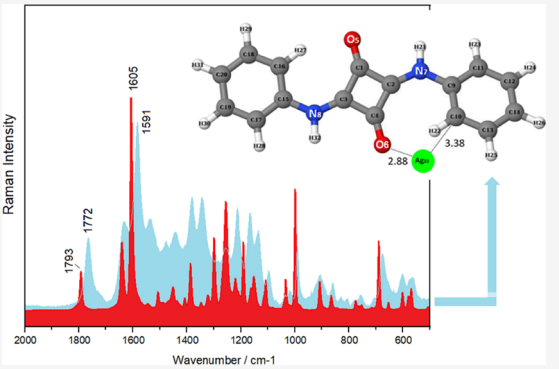

1. INTRODUCTION

Squaraine-based dyes are a class of organic compounds with diverse uses in different fields of science, from organic synthesis to modern applications, such as photodynamic therapy,[1−3] molecular sensors,[4−9] and imaging,[1,8−10] and as photoinitiators of polymerization reactions.[11] Several of these fascinating derivatives present important nitrogen-containing groups inserted in the ring, generating improved systems with new or upgraded properties. This is essentially due to their excellent thermal and photochemical stabilities,[12] besides their peculiar absorption and emission features.[13−15] Thus, many squaraine-based dyes have been extensively investigated and vibrational spectroscopies also emerge as a potential tool for their investigation together with other techniques such as fluorescence-based detection.[1,8,16−19] Such species are normally known as squaraine, squarylium, or squaramide compounds, and there are several derivatives available in the literature.[19−21]

1,3-Dianiline squarate (DSQ) or also called 1,3-bis-(phenylamino)squaraine (**1**) is a symmetric molecule presenting a resonance stabilized structure (see Scheme 1). It is composed of a highly electron-deficient central core (from the oxocarbon squarate, SQ, **2**), surrounded by two opposite "aniline" ligands, electron-rich donating species, forming a *trans*-zwitterionic structure with important spectroscopic

Scheme 1. Chemical Structure of Zwitterionic Structures of DSQ: 1,3-Dianiline Squarate or *trans*-Bis(phenylamino)squaraine (1a/1b) and the Precursor Squaric Acid (2)

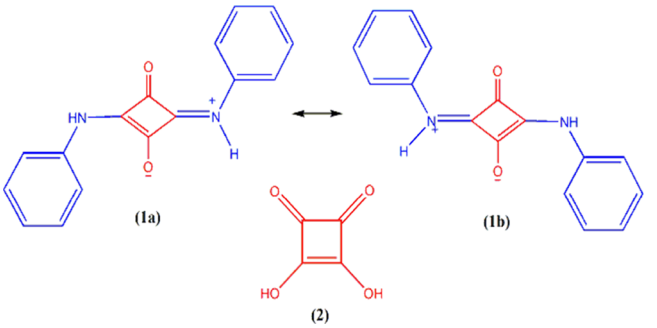

Received: October 9, 2022
Revised: November 30, 2022
Published: December 27, 2022

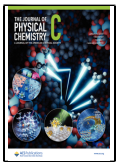

https://doi.org/10.1021/acs.jpcc.2c07109
J. Phys. Chem. C 2023, 127, 421−428

implications. SQ is powerful electrophilic species and reacts easily with aromatic amines yielding deeply colored condensation products.[22,23] DSQ has been commonly used as an intermediary reactant aiming to obtain 1,3-(R_1R_2)-squarate derivatives.[24−28] However, its specific potential applications have been underexplored despite some studies dating back to 1975, possibly due to its solubility issues.[29,30] There are not many studies available in the literature about its physical−chemical properties, and only a few characterization data can be found.[24,25,31]

Although the practical uses of DSQ and DSQ-based dyes have been sparse, in the last few years, there has been increasing attention to their applications as photosensitizers.[11,32,33] Due to their strong light absorption in the blue region, these squaraines have been used as visible light photoinitiators in photopolymerization reactions.[11,32] Compared with some commercially available photoinitiators, DSQ-based systems can lead to better polymerization efficiencies.[32,33] In this regard, Kabatc et al. have demonstrated that the photo-excited squaraine might act both as an electron donor or acceptor, simply changing the co-initiator.[33] Other optical spectroscopic properties of DSQ-based dyes were recently found by Vega et al. and ensure further potential applications.[34] In their work, it was observed that the monoanion of 1,3-bis(4-cyanophenylamino) squaraine shows intense fluorescence in the presence of silver ions. Here, we aim to study the adsorption of DSQ on silver nanoparticles. To the best of our knowledge, this is the first study that explores such species both experimental and theoretically by using a combination of surface-enhanced Raman scattering (SERS) and density functional theory (DFT) calculations. SERS is a highly selective and sensitive spectroscopic technique suitable to study the molecule on an extraordinary scale, making it possible to get convenient information, such as the molecule interactions and/or orientation on the nanoparticle surfaces.[35,36] SERS studies of some oxocarbons, pseudo-oxocarbons, and squaraine derivatives have been widely carried out before; for example, Stokes et al. studied the SERS properties of several squaraine dyes and showed that they are excellent SERS reporters in the red and near-infrared spectral region.[37−43] SERS of squaraines has also found important applications in studies related to cancer diagnosis and imaging,[9,43] which makes this study an important complement to understanding their chemical behavior.

2. MATERIALS AND METHODS

2.1. Synthesis. All chemical reagents were of analytical grade, obtained from commercial suppliers, and used as received. Aniline was previously bi-distilled and squaric acid (SQ) was used without pretreatment, both chemicals from Sigma-Aldrich (Merck). DSQ was synthesized according to adaptations in the methodology available in the literature.[24,25,28,44,45] *N*,*N*-Dimethylformamide (DMF) was predried with molecular sieves. Diamidation reaction was conducted under a boiling solvent point for 100 min; the mixture of 0.570 g (5 mmol) of SQ in 25 mL of DMF was added to 0.930 g (10 mmol) of aniline (molar ratio 1:2). After this period was added 15 mL of water at 5 °C to stop the process; the yellow product obtained was purified by washing with the following solvent gradients and temperatures (two times): water at 50 °C, acetonitrile, hot methanol (60 °C), acetone, and dichloromethane (25 °C). A second purification was necessary by adding DMF at 50 °C under stirring for 1 h. Yield 86%. Anal. calc for C16H12O2N2.1DMF: C, 72.72; H, 4.58; N, 10.60%. Found: C, 69.52; H, 4.88; N, 11.42%. Solid 13C nuclear magnetic resonance (NMR) (ppm): 260.2 (C1), 248.8 (C3), 241.0(C2), 238.7(C4), 177.5, 170.6(C9/C15), 167.9(C12/C13), 140.7(C18/C19/C20), 121.7(C16/C17), 129.5(C14), 119.2(C10/C11), 40.9, 37.9.

2.2. Colloid Preparation. The silver colloid was prepared according to Creighton's chemical reduction method.[46] Briefly, 30 mL of sodium borohydride solution (2.0 mM) was placed in an ice bath under vigorous stirring, and then, 20 mL of $AgNO_3$ (1.0 mM) was added dropwise. The stock solution of 50 mM DSQ was prepared in dimethyl sulfoxide. For the SERS experiments, 5 μL of the stock solution of DSQ was added to 0.5 mL of the silver colloid. The final concentration of DSQ was 495 μM.

2.3. Vibrational Techniques. The SERS spectrum was recorded using a portable Raman spectrometer (Enwave Optronics, Inc.) with a 532 nm excitation wavelength, 20 mW laser power at the sample, and 20 s exposure time. The shown spectrum corresponds to the average of five spectral scans. The Fourier-transform Raman spectrum was obtained by using a Bruker MultiRAM instrument equipped with a Nd^{3+}/YAG laser of 1064 nm wavelength. The final spectrum was obtained by accumulating 512 scans, with a 4 cm^{-1} spectral resolution and 50 mW laser power. The infrared spectrum was obtained by using a Bruker Alpha FTIR spectrometer with a diamond ATR crystal using the accumulation of 128 spectral scans with 4 cm^{-1} spectral resolution.

All calculations were performed on cluster GAUSS of INCT-FCx using the Gaussian 09 program.[47] The Raman activities and infrared (IR) intensities of DSQ and its silver complex (Ag−DSQ) in a vacuum were calculated by the following procedure: first, full geometry optimizations were performed using the CAM-B3LYP functional[48] with the basis set def2TZVP, and then, the vibrational wavenumbers, Raman activities, and IR intensities were obtained. The vibrational analysis confirmed the equilibrium geometries of all studied structures, and no imaginary wavenumbers were observed in the calculated spectra. The atomic charges calculated with CHELPG using the same level of QM calculation.[49]

2.4. NMR Measurements. NMR spectra were performed on a Bruker Avance III HD300 (7.04 T) spectrometer at 75 MHz for ^{13}C in which a 4 mm inverse probe head was installed (ZrO_2 MAS rotors with KeI-F caps). The chemical shift was referenced indirectly by using glycine as an external reference, and tetramethylsilane as the primary standard.

3. RESULTS AND DISCUSSION

The structure of DSQ is auxiliary, confirmed from its ^{13}C NMR spectrum as shown in Figure S1 of the Supplementary Material. Despite all the complexity of this system, there are 10 sets of carbon atoms present in the resonance spectrum. Four non-equivalent carbonyl carbons (C1 to C4) resonate up δ 230 ppm, all of them from the squaryl group; that is, important information once shows the diverse chemical environment of each SQ-carbon. That information is essential to evaluate the preferential interaction with other groups as will be discussed next. The carbons from the phenyl groups, despite similarities, show slight differences at resonance shifts due to the positive charge located preferentially at one nitrogen atom. This promotes different levels of charge delocation around that specific phenyl-carbon, and then, we can verify some

https://doi.org/10.1021/acs.jpcc.2c07109
J. Phys. Chem. C 2023, 127, 421−428

equivalent resonance as C10 and C11 at δ 119 ppm. Other equivalent carbon resonance signals can be assigned as C16/C17 at δ 122 ppm; C18/C19 and C20 at δ 141 ppm; and C12/C13 at δ 168 ppm. In the region up to 235 ppm are the resonances of carbons from the squaryl carbons: C4, C2, C3, and C1 at δ 239, 241, 249, and 260 ppm, respectively. These carbons atoms are not in a similar chemical environment and, therefore, appear as different peaks with low intensity and are severely unshielded. Such species are strongly influenced by their position between the two opposite aniline groups, which will pull the electron density toward it and causes the deshielding of these nuclei.

The normal Raman and IR spectra of solid DSQ are shown in Figure 1. The calculated optimized structure of the isolated

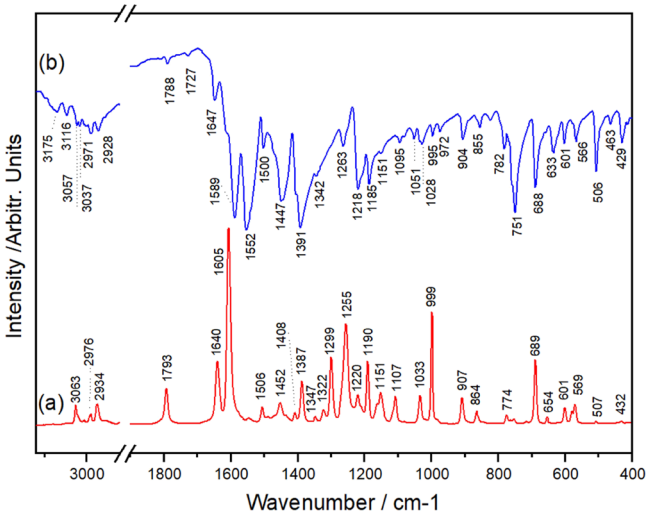

Figure 1. (a) Normal Raman and (b) IR spectra of solid DSQ.

DSQ is shown in Figure 2a, and the structural parameters can be found in Tables S1 and S2. Tables 1 and S3 list the experimental Raman and IR wavenumbers of solid DSQ, the

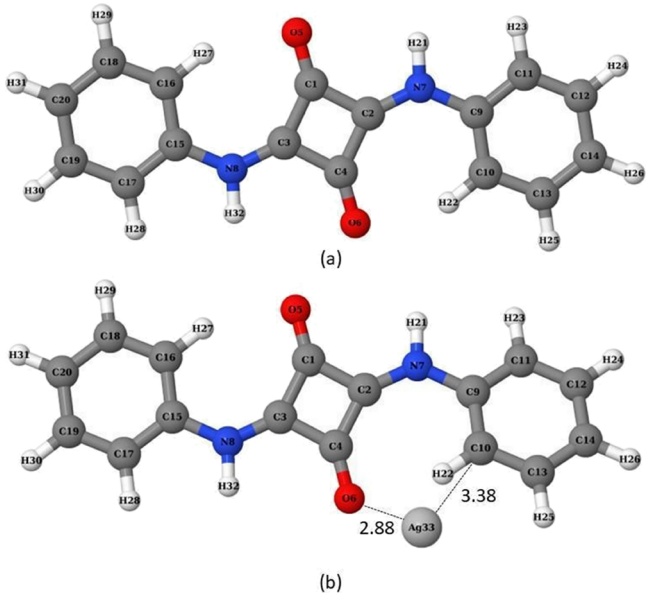

Figure 2. Optimized structures of (a) DSQ and (b) Ag–DSQ complex. The distances are in Å.

calculated wavenumbers, Raman activities, and IR intensities, as well as the corresponding vibrational mode assignments. The vibrational assignments were carried out based on the DFT calculations and in the literature data available for aniline and its derivatives.[50,51] We used as criteria for the vibrational assignment, the correlation between the calculated wavenumbers, Raman activity, and IR intensities with the observed spectra. There is in general an excellent agreement between the non-scale predicted wavenumbers with the experimental Raman and IR band positions. The major differences occur above 1600 cm^{-1} where a theoretical scaling factor would improve the match between the experiment and calculation. There are some discrepancies in the calculated and experimental relative intensity. However, the predicted presence of Raman and IR active peaks in some specific spectral regions was useful for more reliable band assignments.

The most intense bands in the normal Raman spectrum of solid DSQ occur at 689, 999, 1255, and 1605 cm^{-1}. The Raman band detected at 999 cm^{-1} is assigned to the phenyl ring breathing vibrations. The band at 1255 cm^{-1} has a contribution from in-plane C–H bending, N–H bending, and C–N stretching modes. The strongest Raman band observed at 1605 cm^{-1} is assigned to a mixture of in-plane phenyl ring stretching, C–H bending, and C–N stretching vibrations. The IR spectrum of solid DSQ matches well with the one previously reported by Gauger and Manecke[29] The strongest bands are observed at 688, 751, 1391, 1552, and 1589 cm^{-1}; the bands at 751 and 1391 cm^{-1} are assigned to out-of-plane and in-plane C–H bending from phenyl groups, respectively. The band at 751 cm^{-1} also has a contribution from N–H out-of-plane bending. The bands at 1552 and 1589 cm^{-1} correspond to a combination of in-plane C–H and N–H bending movements.

The analysis of both the absorption and scattering spectra highlights the IR active band at 1552 cm^{-1}; as above-mentioned, it is assigned to the in-plane asymmetric vibrations of phenyl groups. Other peaks relatively strongest in the IR than in the Raman spectrum can be observed at 751, 1391, and 1447 cm^{-1}; with exception of the first one (assigned to out-of-plane vibrations), the others are assigned to in-plane vibrations from phenyl (δCH/NH) and squarate groups (νCN). The strongest Raman bands can be found at 999 and 1255 cm^{-1}; both have the contribution of phenyl groups, the first mode contains the phenyl rings breathing, and the second vibration includes deformations of CH/NH, added to the CN stretching. The peak at 1605 cm^{-1} also deserves to be highlighted once it is the most intense band in the spectrum and has the contribution of important groups from phenyl and SQ. It corresponds to CC phenyl, CO stretching, and νC–N where "C" is from SQ and "N" is from the aniline group. That could be considered a "marker band" once perturbations on this region must impact the energy mode, which could be considered a "key peak".

Several other bands are also observed in the vibrational spectra of solid DSQ. The peak at 1793 cm^{-1} in the normal Raman spectrum corresponds to a combination of C=O and C–N stretching vibrations. This is in agreement with the position of the carbonyl stretching vibration previously reported for the squarate dianion in solution and solid samples.[52] The corresponding band in the IR spectrum occurs at 1788 cm^{-1}, but its intensity is relatively very weak.

The bands at 429 and 506 cm^{-1} have a contribution from phenyl rings and C–H out-of-plane bending. The band at 782

https://doi.org/10.1021/acs.jpcc.2c07109
J. Phys. Chem. C 2023, 127, 421–428

Table 1. Summary of Band Positions for Normal Raman and Infrared Spectra of DSQ (Solid) and SERS (495 μM) of DSQ; Calculated Data, Raman Activities, and IR Intensities of DSQ and the Ag−DSQ Complex[a]

		calculation DSQ					calculation Ag−DSQ			
FT-Raman (cm^{-1})	FT-IR (cm^{-1})	cm^{-1}	Raman act. ($Å^4$/amu)	IR int. (km/mol)	DSQ assignments	SERS (cm^{-1})	cm^{-1}	Raman act. ($Å^4$/amu)	IR int. (km/mol)	Ag−DSQ assignments
414 vvw	414 vw	424.0	0	0	ωR1/ωR2/ωCH(R1,R2)	411 vw	422.7	0.1	0.0	ωR2/ωCH(R2)
432 vw	429 m	424.1	0	0	ωR1/ωR2/ωCH(R1,R2)	442 vvw	426.8	4.6	0.1	ωR1/ωCH(R1)
	463 w	474.1	0	27.0	δR1/δR2/δCO/δCCN		475.2	0.5	26.3	δR1/δR2/δCO/δCCN
507 vw		522.8	3.9	0	ωR1/ωR2/ωCH(R1,R2)	514 vw sh	523.5	4.3	4.1	ωR1/ωR2/ωCH(R1,R2)
	506 s	531.3	0	26.9	ωR1/ωR2/ωCH(R1,R2)		530.6	1.1	29.4	ωR1/ωR2/ωCH(R1,R2)
569 w	566 m	545.0	3.7	0	ωNH/ωSq		557.9	28.5	4.8	ωNH/ωSq
	601 m	618.5	0	13.8	δR1/δR2/δCNC		619.8	0.87	11.2	δR1/δR2/δCNC
601 w		629.7	35.4	0	δR1/δR2	612 w	631.8	28.7	0.0	δR1/δR2
	633 m	640.3	0	0.3	δR1/δR2		641.9	0.4	0.2	δR1/δR2
654 vw		663.8	3.3	0	δSq/δR1/δR2	667 sh	666.8	4.7	1.1	δSq/δR1/δR2
689 s	688 s	690.7	0.2	0	ωSq/ωNH	686 s	691.8	1.5	2.3	ωSq/ωNH
		716.3	24.0	0	δSq/δR1/δR2	718 vw sh	718.1	17.0273	4.3	δSq/δR1/δR2
752 vw	751 s	718.1	0	98.4	ωCH(R1,R2)/ωNH	764 vw	721.8	2.0	54.3	ωCH(R1)/ωNH
	782 m	785.1	0	136.4	ωCH(R1,R2)		787.1	1.7	79.0	ωCH(R2)
907 m	904 m	918.1	39.5	0	δCCN	917 m	920.7	33.1	0.2	δCCN
	995 w	1026.4	0.4	2.0	ring breathing (R1,R2)		1031.1	77.1	1.6	ring breathing (R2)
999 s		1026.8	276.2	0	ring breathing (R1,R2)	999 s	1032.2	186.8	0.3	ring breathing (R1)
1033 m		1068.1	101.3	0	δCH(R1,R2)	1028 vw	1071.9	79.8	0.0	δCH(R1,R2)
	1028 m/ 1051 w	1070.7	0	0.9	δCH(R1,R2)	1045 vw	1074.6	1.6	0.2	δCH(R1,R2)
1107 m		1130.0	10.6	0	δCH(R1,R2)	1104 m	1134.9	8.4	0.5	δCH(R1,R2)
1151 m		1179.5	63.0	0	δCH(R1,R2)/δNH1/δNH2/δSq	1144 m	1184.7	27.6	54.5	δCH(R2)/δNH2/δSq
	1185 m	1188.6	0	7.0	δCH(R1,R2)		1196.6	1.66	1.9	δCH(R1,R2)
1190 m		1189	73.4	0	δCH(R1,R2)	1175 s	1196.9	51.2	0.8	δCH(R1,R2)
1220 m		1226.2	289.1	0	δCH(R1,R2)	1220 s	1231.8	141.5	0.8	δCH(R1)
	1218 s	1227.6	0	0.9	δCH(R1,R2)		1234.9	93.9	0.1	δCH(R2)
1255 s		1270.5	2501.0	0	δCH(R1,R2)/δNH1/δNH2/νCN	1262 m	1275.3	2137.4	0.5	δCH(R1,R2)/δNH1/δNH2/νCN
1299 m	1263 m	1281.5	0	51.0	δCH(R1,R2)/δNH1/δNH2/νCN	1307 w	1285.9	68.8	47.0	δCH(R1,R2)/δNH1/δNH2/νCN
1323 w/ 1346 vw		1333.8	476.8	0	δCH(R1,R2)/νR1/νR2	1351 s	1335.1	352.8	2.3	δCH(R1)/νR1
	1391 s	1384.9	0	273.5	δCH(R1,R2)		1388.4	11.4	168.5	δCH(R1)
1387 s		1387.5	96.1	0	δCH(R1,R2)	1389 s	1392.9	64.8	71.9	δCH(R2)
1452 w	1447 s	1429.0	0	2853.2	δNH1/δNH2/νCN	1450 m	1431.4	2.4	2531.5	δNH1/δNH2/νCN
		1488.0	84.0	0	δCH(R1,R2)/δNH1/δNH2	1487 m	1490.4	75.9	3.2	δCH(R1,R2)/δNH1/δNH2
	1500 m	1497.1	0	393.2	δCH(R1,R2)/δNH1/δNH2		1501.5	5.7	429.4	δCH(R1,R2)/δNH1/δNH2
	1552 s	1552.2	0	39.3	δCH(R1,R2)/δNH1/δNH2		1558.4	22.5	21.8	δCH(R1,R2)/δNH1/δNH2
1546 vw		1554.6	380.2	0	δCH(R1,R2)	1540 s	1560.9	308.6	1.8	δCH(R1,R2)
	1589 s	1583.8	0	1635.2	δNH1/δNH2/δCH(R1,R2)		1583.9	3.3	1482.9	δNH1/δNH2/ δCH (R1,R2)
1605 vs		1661.5	554.9	0	δCH(R1,R2)/νR1/νR2/νCN/CO	1591 vs	1659.9	522.2	119.2	δCH(R1,R2)/νR1/νR2/νCN/CO
	1613 sh	1675.2	0	159.9	δCH(R1,R2)/νR1/νR2/δNH		1676.0	13.3	152.9	δCH(R1,R2)/νR1/νR2/δNH

https://doi.org/10.1021/acs.jpcc.2c07109
J. Phys. Chem. C 2023, 127, 421−428

Table 1. continued

		calculation DSQ					calculation Ag−DSQ			
FT-Raman (cm^{-1})	FT-IR (cm^{-1})	cm^{-1}	Raman act. ($Å^4$/amu)	IR int. (km/mol)	DSQ assignments	SERS (cm^{-1})	cm^{-1}	Raman act. ($Å^4$/amu)	IR int. (km/mol)	Ag−DSQ assignments
1640 s	-	1681.8	2542.1	0	δCH(R1,R2)/νR1/νR2/δNH	1629/1646 s	1684.0	1635.4	14.9	δCH(R1,R2)/νR1/νR2/δNH
	1647 m	1682.4	0	40.0	δCH(R1,R2)/νR1/νR2/δNH		1685.6	283.4	49.6	δCH(R1,R2)/νR1/νR2/δNH
	1727 vw	1721.1	0	1393.8	νCO	1729 sh	1713.9	107.0	945.9	νCO/νCN/δNH
1793 s	1788 vw	1893.7	91.7	0	νCO/νCN	1772 s	1889.6	167.0	10.6	νCO/νCN
2934 w	2928 w	3182.2	52.0	2.4	νCH(R1)	2925 m	3184.1	36.1	6.0	νCH(R2)
2976 w	2971 w	3182.3	15.9	7.8	νCH(R2)		3186.7	42.0	5.4	νCH(R1)
3063 w		3207.2	194.6	0	νCH(R1,R2)	3064 w	3210.9	82.0	7.2	νCH(R2)
	3116 w	3219.0	1.1	35.1	νCH(R1,R2)		3222.9	377.0	18.5	νCH(R2)
	3175 w	3565.5	0.2	145.4	νNH		3552.5	119.4	93.7	νNH

[a]ν, stretching; δ, in-plane bending; ω, out-of-plane bending; τ, twisting; Sq, squaryl ring; R1, phenyl ring 1; R2, phenyl ring 2; sh, shoulder; s, strong; m, medium; w, weak; v, very.

cm^{-1} is assigned to C−H out-of-plane bending. The peak at 688 cm^{-1} is a combination of the squaryl and N−H out-of-plane bending. In the Raman spectrum, except for the band at 689 cm^{-1}, the other out-of-plane vibrations are weak.

The SERS spectrum of DSQ using silver nanoparticles is shown in Figures 3, S2, and S3. Table 1 summarizes the

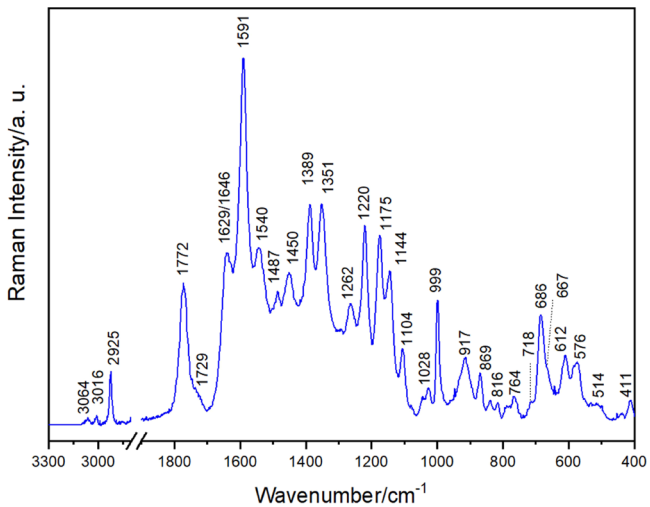

Figure 3. SERS spectrum of DSQ using 532 nm excitation.

wavenumbers of the observed bands, the calculated wavenumbers, Raman activities, and IR intensities, as well as the corresponding vibrational mode assignments obtained using the Ag(0)−DSQ model shown in Figure 2b. Other predicted data can be found in Tables S1 and S2. The SERS spectrum of DSQ is crowded in the spectral region from 1000 to 1700 cm^{-1} (Figure S2 shows the spectral deconvolution of the SERS spectrum). Though the number of active bands agrees well with those detected in the normal Raman spectrum of the solid sample, several differences are observed in their positions and relative intensities. Figure S3 shows the similarities between both normal Raman and SERS spectra of DSQ; the stronger band in the SERS spectrum at 1591 cm^{-1} corresponds to the stronger band of the solid but is shifted −14 cm^{-1}; as expected, this band is a good peak marker in the sense of monitoring the environment around the linked regions between SQ and aniline groups. Bands at 1144, 1220, 1351, 1540, and 1772 cm^{-1} are remarkably enhanced in the SERS spectrum compared with the normal Raman of the solid, all of them assigned to in-plane vibrational movements.

The carbonyl stretching band at 1793 cm^{-1} in the solid sample shifts to 1772 cm^{-1} in the SERS spectrum. In previous work, the SERS spectrum of SQ has a very strong band at 1772 cm^{-1}.[42] It was suggested that the intensity enhancement of this mode is due to the adsorption of the oxocarbon on the nanoparticle surface through the carbonyl oxygen. Therefore, the presence of this strong band in the SERS spectrum of DSQ is an essential indicator of its adsorption, which may occur through one of the oxygen atoms. This interpretation is also supported by the optimized structure of the Ag(0)−DSQ complex since there is favorable coordination of the silver atom to one oxygen of the squaryl ring (see Figure 2b). As shown in Table S2, there are only small changes in the bond distances and angles in the presence of a silver atom. However, there is a slight lengthening of the C_4−O_6 bond which may explain the

https://doi.org/10.1021/acs.jpcc.2c07109
J. Phys. Chem. C 2023, 127, 421−428

wavenumber downshift of the carbonyl stretching band in the SERS spectrum.

Only a few out-of-plane vibrations of DSQ are observed in the SERS spectrum at 411, 686, and 764 cm^{-1}. The bands at 411 and 764 cm^{-1}, which are very weak in the spectrum of the solid, are slightly enhanced in the SERS spectrum. The band at 411 cm^{-1} is assigned to a combination of the phenyl ring and C−H out-of-plane bending. The peak at 764 cm^{-1} is attributed to C−H out-of-plane bending and N−H out-of-plane bending. Qi et al. observed intensity enhancement of these bands in the SERS spectrum of aniline, suggesting that the molecule adopts a tilted orientation on the metal surface.[50] The observed strong SERS intensity of the 686 cm^{-1} band, which has a contribution from squaryl out-of-plane bending, also indicates that the four-membered ring of DSQ may be tilted relative to the nanoparticle surface.

As seen in Figure 2b, the obtained minimum energy geometry of Ag(0)−DSQ is non-planar with the silver atom interacting with one oxygen. Using DFT calculations, Vega et al. also reported a non-planar structure for the complex of deprotonated 1,3-bis(4-cyanophenylamino) squaraine with two silver atoms.[34] It was shown that each silver atom interacts with one phenyl ring by an Ag(I)−π interaction. The DFT calculation of Ag(0)−DSQ carried out here suggests a weak interaction of the Ag atom with one of the phenyl rings sufficiently to perturb the planarity of the DSQ. The calculation predicts a quasi-planar structure for DSQ, with torsion angles of α (C_3−N_8−C_{15}−C_{16}) = −0.002° and β (C_2−N_7−C_9−C_{10}) = −0.035° (demonstrating coplanarity between the two phenyl rings and squaryl ring), and a nonplanar structure for the Ag(0)−DSQ complex with α = 0.103° and β = −14.276°. The band at 907 cm^{-1} in the normal Raman spectrum, which is assigned to C_4−C_3−N_8 and C_1−C_2−N_7 in-plane bending motions, shifts to 917 cm^{-1} in the SERS spectrum. The predicted change in the torsion angle β in the presence of the silver atom explains the experimental shift in the wavenumber of this band.

The interaction of the silver atom with DSQ may also be the origin of the shift of other bands with contribution from C−H vibrations.[53] For instance, the bands at 1151, 1190, 1255, and 1605 cm^{-1} in the normal Raman spectrum shift to 1144, 1175, 1262, and 1591 in the SERS spectrum, respectively. The change in the torsion angle β may have also an influence on the shift of the bands at 1255 and 1605 cm^{-1} which have the contribution of C−N stretching vibrations.

Despite DSQ derivative presenting as a very symmetrical system, NMR data preliminary showed us different carbons atoms from squaryl groups; thus, there were diverse chemical environments available for process adsorptions, but only one of them was favorable for it. Overall, the results obtained here suggest that DSQ is mainly adsorbed through one of the carbonyl groups and has a weak interaction with the silver nanoparticle. They also indicate that the molecule lost its planar structure in the presence of the nanoparticle and has a tilted configuration concerning the surface.

4. CONCLUSIONS

In the present work, we have reported and characterized for the first time the normal Raman and SERS spectra of DSQ. The detailed comparison of these spectra suggests that DSQ has a tilted configuration correlated with the silver nanoparticle surface. From the experiments and the DFT calculations, it was revealed that surface adsorption may occur through the interactions of a DSQ carbonyl group and a phenyl ring with the silver atoms. In addition, the presence of the nanoparticle (silver atom) promoted the loss of planarity of the DSQ structure. Taking into account the known use of squaraines and the results obtained here, it is expected that the interaction of the DSQ and DSQ-based dyes with plasmonic silver nanoparticles can open potential applications in several fields and particularly in nanoplasmonics.

■ ASSOCIATED CONTENT

Supporting Information

The Supporting Information is available free of charge at https://pubs.acs.org/doi/10.1021/acs.jpcc.2c07109.

Solid-state ^{13}C NMR spectrum of DSQ; deconvolution of the SERS spectrum of DSQ; Raman spectra; XYZ coordinates; data for the optimized geometries; and band positions for Normal Raman and infrared spectra (PDF)

■ AUTHOR INFORMATION

Corresponding Authors

Vanessa End de Oliveira − *Departamento de Ciências da Natureza, Universidade Federal Fluminense, 28895-532 Rio das Ostras, Rio de Janeiro, Brazil;* orcid.org/0000-0002-6294-4782; Email: vanessaend@id.uff.br

Erix Alexander Milán-Garcés − *Departamento de Física Geral, Instituto de Física, Universidade de São Paulo, 05508-090 São Paulo, São Paulo, Brazil*; Email: garces@usp.br

Authors

Antônio Rodrigues da Cunha − *Universidade Federal do Maranhão, 65800-000 Maranhão, Brazil*

Márcia de Almeida Rizzutto − *Departamento de Física Nuclear, Instituto de Física, Universidade de São Paulo, 05508-090 São Paulo, São Paulo, Brazil*

Maria Teresa Lamy − *Departamento de Física Geral, Instituto de Física, Universidade de São Paulo, 05508-090 São Paulo, São Paulo, Brazil;* orcid.org/0000-0001-6616-6546

Luiz Fernando Cappa de Oliveira − *Núcleo de Espectroscopia e Estrutura Molecular, Departamento de Química, Instituto de Ciências Exatas, Universidade Federal de Juiz de Fora, 36036-900 Juiz de Fora, Minas Gerais, Brasil*

Complete contact information is available at: https://pubs.acs.org/10.1021/acs.jpcc.2c07109

Notes

The authors declare no competing financial interest.

■ REFERENCES

(1) Beverina, L.; Salice, P. Squaraine Compounds: Tailored Design and Synthesis towards a Variety of Material Science Applications. *Eur. J. Org. Chem.* **2010**, *2010*, 1207−1225.

(2) Magalhães, Á. F.; Graça, V. C.; Calhelha, R. C.; Ferreira, I. C. F. R.; Santos, P. F. Aminosquaraines as potential photodynamic agents: Synthesis and evaluation of in vitro cytotoxicity. *Bioorg. Med. Chem. Lett.* **2017**, *27*, 4467−4470.

(3) Ramaiah, D.; Eckert, I.; Arun, K. T.; Weidenfeller, L.; Epe, B. Squaraine Dyes for Photodynamic Therapy: Study of Their Cytotoxicity and Genotoxicity in Bacteria and Mammalian Cells. *Photochem. Photobiol.* **2002**, *76*, 672−677.

(4) Ananda Rao, B.; Kim, H.; Son, Y.-A. Synthesis of near-infrared absorbing pyrylium-squaraine dye for selective detection of Hg2+. *Sens. Actuators B Chem.* **2013**, *188*, 847−856.
(5) Huang, Y.; Lin, Q.; Wu, J.; Fu, N. Design and synthesis of a squaraine based near-infrared fluorescent probe for the ratiometric detection of Zn2+ ions. *Dyes Pigm.* **2013**, *99*, 699−704.
(6) McEwen, J. J.; Wallace, K. J. Squaraine dyes in molecular recognition and self-assembly. *Chem. Commun.* **2009**, *42*, 6339−6351.
(7) Ramroop-Singh, N.; Narinesingh, D.; Singh, G.; Seto, C. T.; Comeau, A. B. The binding site of zinc and indium metal to amino acid derivatized squarate complexes â€“ Implications in inhibitor and mediator designs. *Bioorg. Chem.* **2010**, *38*, 234−241.
(8) Liu, X.-D.; Sun, R.; Ge, J.-F.; Xu, Y.-J.; Xu, Y.; Lu, J.-M. A squaraine-based red emission off-on chemosensor for biothiols and its application in living cells imaging. *Org. Biomol. Chem.* **2013**, *11*, 4258−4264.
(9) Narayanan, N.; Karunakaran, V.; Paul, W.; Venugopal, K.; Sujathan, K.; Kumar Maiti, K. Aggregation induced Raman scattering of squaraine dye: Implementation in diagnosis of cervical cancer dysplasia by SERS imaging. *Biosens. Bioelectron.* **2015**, *70*, 145−152.
(10) McAughtrie, S.; Faulds, K.; Graham, D. Surface enhanced Raman spectroscopy (SERS): Potential applications for disease detection and treatment. *J. Photochem. Photobiol., C* **2014**, *21*, 40−53.
(11) Giacoletto, N.; Ibrahim-Ouali, M.; Dumur, F. Recent advances on squaraine-based photoinitiators of polymerization. *Eur. Polym. J.* **2021**, *150*, No. 110427.
(12) Gao, F.-P.; Lin, Y.-X.; Li, L.-L.; Liu, Y.; Mayerhöffer, U.; Spenst, P.; Su, J.-G.; Li, J.-Y.; Würthner, F.; Wang, H. Supramolecular adducts of squaraine and protein for noninvasive tumor imaging and photothermal therapy in Â vivo. *Biomaterials* **2014**, *35*, 1004−1014.
(13) Paternò, G. M.; Galliano, S.; Barbero, N.; Barolo, C.; Borrelli, R.; Lanzani, G.; Scotognella, F. Spectroscopic investigation of squaraine dyes. In *Proc.SPIE*, 2017, 10101.
(14) Shafeekh, K. M.; Das, S.; Sissa, C.; Painelli, A. Asymmetric Squaraine Dyes: Spectroscopic and Theoretical Investigation. *J. Phys. Chem. B* **2013**, *117*, 8536−8546.
(15) Sreejith, S.; Carol, P.; Chithra, P.; Ajayaghosh, A. Squaraine dyes: a mine of molecular materials. *J. Mater. Chem.* **2008**, *18*, 264−274.
(16) Law, K.-Y. Squaraine Chemistry. Absorption, Fluorescence Emission, and Photophysics of Unsymmetrical Squaraines. *J. Phys. Chem.* **1995**, *99*, 9818−9824.
(17) Radaram, B.; Mako, T.; Levine, M. Sensitive and selective detection of cesium via fluorescence quenching. *Dalton Trans.* **2013**, *42*, 16276−16278.
(18) Wu, I. C.; Yu, J.; Ye, F.; Rong, Y.; Gallina, M. E.; Fujimoto, B. S.; Zhang, Y.; Chan, Y.-H.; Sun, W.; Zhou, X.-H.; et al. Squaraine-Based Polymer Dots with Narrow, Bright Near-Infrared Fluorescence for Biological Applications. *J. Am. Chem. Soc.* **2015**, *137*, 173−178.
(19) Lim, N. C.; Pavlova, S. V.; Brückner, C. Squaramide Hydroxamate-Based Chemidosimeter Responding to Iron(III) with a Fluorescence Intensity Increase. *Inorg. Chem.* **2009**, *48*, 1173−1182.
(20) Merritt, V. Y.; Hovel, H. J. Organic solar cells of hydroxy squarylium. *Appl. Phys. Lett.* **1976**, *29*, 414−415.
(21) Ian Storer, R.; Aciro, C.; Jones, L. H. Squaramides: physical properties, synthesis and applications. *Chem. Soc. Rev.* **2011**, *40*, 2330−2346.
(22) Sprenger, H.-E.; Ziegenbein, W. Condensation Products of Squaric Acid and Tertiary Aromatic Amines. *Angew. Chem., Int. Ed. Engl.* **1966**, *5*, 894−894.
(23) Sprenger, H. E.; Ziegenbein, W. Cyclobutenediylium Dyes. *Angew. Chem., Int. Ed. Engl.* **1968**, *7*, 530−535.
(24) de Oliveira, V. E.; de Carvalho, G. S.; Yoshida, M. I.; Donnici, C. L.; Speziali, N. L.; Diniz, R.; de Oliveira, L. F. C. Bis-(dicyanomethylene)squarate squaraines in their 1,2- and 1,3-forms: Synthesis, crystal structure and spectroscopic study of compounds containing alkali metals and tetrabutylammonium ions. *J. Mol. Struct.* **2009**, *936*, 239−249.
(25) de Oliveira, V. E.; Freitas, M. C. R.; Diniz, R.; Yoshida, M. I.; Speziali, N. L.; Edwards, H. G. M.; de Oliveira, L. F. C. Crystal structure and vibrational spectra of some metal complexes of pseudo-oxocarbon bis(dicyanomethylene)squarate in its cis and trans forms. *J. Mol. Struct.* **2008**, *881*, 57−67.
(26) de Oliveira, V. E.; Diniz, R.; de Oliveira, L. F. C. Oxocarbons, Pseudo-oxocarbons, and Squaraines. *Quim. Nova* **2009**, *32*, 1917−1925.
(27) Silva, C. E.; Diniz, R.; Rodrigues, B. L.; de Oliveira, L. F. C. Crystal structure and spectroscopic analysis of the asymmetric squaraine [(2-dimethylamino-4-anilino)squaraine]. *J. Mol. Struct.* **2007**, *831*, 187−194.
(28) Lunelli, B.; Monari, M.; Bottoni, A. Geometry, Energy, and Vibrational Frequencies of the Bis(dicyanomethylene)squarilium Dianion. *J. Phys. Chem. A* **2001**, *105*, 2257−2265.
(29) Gauger, J.; Manecke, G. Kondensationsprodukte der Quadratsäure mit primären und sekundären Aminen, I. *Chem. Ber.* **1970**, *103*, 2696−2706.
(30) Neuse, E. W.; Green, B. R. Dianilino derivatives of squaric acid. *J. Org. Chem.* **1974**, *39*, 3881−3887.
(31) Kabatc, J.; Kostrzewska, K.; Jurek, K.; Dobosz, R.; Orzeł, Ł. 1,3-Bis(phenylamino)squaraine â€“ Photophysical and photochemical properties. *Dyes Pigm.* **2016**, *127*, 179−186.
(32) Kostrzewska, K.; Ortyl, J.; Dobosz, R.; Kabatc, J. Squarylium dye and onium salts as highly sensitive photoradical generators for blue light. *Polym. Chem.* **2017**, *8*, 3464−3474.
(33) Kabatc, J.; Kostrzewska, K.; Jurek, K.; Kozak, M.; Balcerak, A.; Orzeł, Ł. New Squaraine-based two-component initiation systems for UV-blue light induced radical polymerization: Kinetic and time-resolved laser spectroscopy studies. *J. Polym. Sci., Part A: Polym. Chem.* **2017**, *55*, 471−484.
(34) Vega, M.; Blasco, S.; García-España, E.; Soberats, B.; Frontera, A.; Rotger, C.; Costa, A. Dual role of silver in a fluorogenic N-squaraine probe based on Ag-π interactions. *Dalton Trans.* **2021**, *50*, 9367−9371.
(35) Jeanmaire, D. L.; Van Duyne, R. P. Surface raman spectroelectrochemistry: Part I. Heterocyclic, aromatic, and aliphatic amines adsorbed on the anodized silver electrode. *J. Electroanal. Chem. Interfacial Electrochem.* **1977**, *84*, 1−20.
(36) Ru, E. C. L.; Etchegoin, P. G. *Principles of Surface Enhanced Raman Spectroscopy: and Related Plasmonic Effects*; Elsevier, 2009.
(37) Alves, A. P. P.; de Sena, L. Á.; Archanjo, B. S.; de Oliveira, L. F. C.; de Oliveira Dantas, S.; Sant'Ana, A. C. Surface-enhanced Raman scattering study of the adsorption of croconate violet on colloidal silver particles. *Vib. Spectrosc.* **2013**, *64*, 153−157.
(38) Milán-Garcés, E. A.; Georgopoulos, S. L.; Barros Santos, P.; Sato, F.; Sant'Ana, A. C.; Andrade, G. F. S.; de Oliveira, L. F. C. Probing ring contraction and decarboxylation of Rhodizonate and the influence of Cu (II) using surface-enhanced Raman Scattering. *J. Raman Spectrosc.* **2020**, *51*, 256−263.
(39) Milán-Garcés, E. A.; Georgopoulos, S. L.; Sant'Ana, A. C.; Andrade, G. F. S.; de Oliveira, L. F. C. Chemical behavior of croconic acid coordinated to Co(II) adsorbed on silver surface. *J. Raman Spectrosc.* **2018**, *49*, 1174−1183.
(40) Stokes, R. J.; Ingram, A.; Gallagher, J.; Armstrong, D. R.; Smith, W. E.; Graham, D. Squaraines as unique reporters for SERRS multiplexing. *Chem. Commun.* **2008**, *5*, 567−569.
(41) Sant'Ana, A. C.; de Siqueira, L. J. A.; Santos, P. S.; Temperini, M. L. A. Vibrational characterization of poly(1-methylpyrrole- co-squaric acid) and poly(1-dodecylpyrrole-co-squaric acid) by enhanced Raman spectroscopy. *J. Raman Spectrosc.* **2006**, *37*, 1346−1353.
(42) Georgopoulos, S. L.; Milán-Garcés, E. A.; Sant'Ana, A. C.; Souza Andrade, G. F.; de Oliveira, L. F. C. Analysis of squaric acid and its complex with copper(II) ions adsorbed on silver nanoparticle surfaces by surface-enhanced Raman spectroscopy. *Vib. Spectrosc.* **2016**, *87*, 99−103.
(43) Ramya, A. N.; Samanta, A.; Nisha, N.; Chang, Y.-T.; Maiti, K. K. New insight of squaraine-based biocompatible surface-enhanced

https://doi.org/10.1021/acs.jpcc.2c07109
J. Phys. Chem. C 2023, 127, 421−428

Raman scattering nanotag for cancer-cell imaging. *Nanomedicine* **2015**, *10*, 561−571.
(44) Farnia, G.; Lunelli, B.; Marcuzzi, F.; Sandonã, G. Dicyanomethylene derivatives of squaric acid: electrochemical behaviour and ESR investigation. *J. Electroanal. Chem.* **1996**, *404*, 261−269.
(45) Doane, L. M.; Fatiadi, A. J. Electrochemical oxidation of several oxocarbon salts in N,N-dimethylformamide. *J. Electroanal. Chem. Interfacial Electrochem.* **1982**, *135*, 193−209.
(46) Creighton, J. A.; Blatchford, C. G.; Albrecht, M. G. Plasma resonance enhancement of Raman scattering by pyridine adsorbed on silver or gold sol particles of size comparable to the excitation wavelength. *J. Chem. Soc., Faraday Trans. 2* **1979**, *75*, 790−798.
(47) *Gaussian 16 Rev. C.01*; Wallingford, CT, accessed.
(48) Yanai, T.; Tew, D. P.; Handy, N. C. A new hybrid exchange-correlation functional using the Coulomb-attenuating method (CAM-B3LYP). *Chem. Phys. Lett.* **2004**, *393*, 51−57.
(49) Breneman, C. M.; Wiberg, K. B. Determining atom-centered monopoles from molecular electrostatic potentials. The need for high sampling density in formamide conformational analysis. *J. Comput. Chem.* **1990**, *11*, 361−373.
(50) Qi, Y.; Hu, Y.; Xie, M.; Xing, D.; Gu, H. Adsorption of aniline on silver mirror studied by surface-enhanced Raman scattering spectroscopy and density functional theory calculations. *J. Raman Spectrosc.* **2011**, *42*, 1287−1293.
(51) Anto, P. L.; Anto, R. J.; Varghese, H. T.; Panicker, C. Y.; Philip, D.; Brolo, A. G. FT-IR, FT-Raman and SERS spectra of anilinium sulfate. *J. Raman Spectrosc.* **2009**, *40*, 1810−1815.
(52) Santos, P. S.; Amaral, J. H.; De Oliveira, L. F. C. Raman spectra of some transition metal squarate and croconate complexes. *J. Mol. Struct.* **1991**, *243*, 223−232.
(53) Yi, H.-B.; Lee, H. M.; Kim, K. S. Interaction of Benzene with Transition Metal Cations: Theoretical Study of Structures, Energies, and IR Spectra. *J. Chem. Theory Comput.* **2009**, *5*, 1709−1717.

https://doi.org/10.1021/acs.jpcc.2c07109
J. Phys. Chem. C 2023, 127, 421−428